Phase Change Materials in a Hybrid Solar Thermal/Photovoltaic Energy Storage System for a Residential House

Xavier Calvão Borges Antunes Ferreira
xavier.ferreira@tecnico.ulisboa.pt

Instituto Superior Técnico, Universidade de Lisboa, Portugal
January 2021

Abstract

Hot water supply has proved to be a subject of great relevance to counter climate change. The integration of solar collectors in residential hot water systems has already been extensively explored, presenting, however, an inconvenient mismatch between energy supply and its consumption. The integration of an energy storage system can counter this obstacle. In this field, phase change materials play an important role, being able to store latent heat. In this thesis, the incorporation of a storage system with phase change materials in a domestic water heating system was investigated. The system proposed in this work consists of a hybrid photovoltaic/thermal solar panel, a water storage tank and a plate heat exchanger with phase change materials. Several configurations were tested and three different phase change materials were studied, with a melting point of around 60 degrees. Simulations were carried out under different climatic conditions, for three different locations: Lisboa, Castelo Branco and Montalegre. The results show that the integration of such a system can lead to a reduction in energy consumption for heating domestic water of around 23% during the summer, and 14% during the winter.
Keywords: Phase change material, plate heat exchanger, residential hot water, energy, latent heat storage.

Nomenclature

TES	Thermal energy storage
PCM	Phase Change Material
SDHW	Solar domestic hot water
PVT	Photovoltaic/thermal
HE	Heat exchanger
PHE	Plate heat exchanger
LNEG	Laboratório Nacional de Energia e Geologia
SC	System configuration

1. INTRODUCTION

The heating and cooling sector comprises a wide spectrum of technologies and applications, ranging from residential to industrial applications. At a global scale, the heating and cooling sector accounts for almost half of the final energy consumption, yet this sector still depends strongly on fossil fuels, contributing to nearly 40% of global energy-related CO2 emissions [1].

Due to the harmful effects on the environment and the non-renewable nature of fossil fuels, focus should shift to alternative sources for power generation. Renewable energy resources, such as solar, present a solution to tackle these issues by providing a more sustainable power generation with much less impact on the environment. However, according to the Global Status Report 2019, only around 25% of the heating and cooling energy demands are met by renewable energy resources [1].

Considering its abundance and reduced costs and environmental impact, solar energy plays an important role in the transition to cleaner energy sources and is already widely implemented around the world. In Portugal, around 60% to 80% of the hot water needs are already supplied by solar thermal collectors [2]. However, the limited sunshine period still remains the main obstacle to this power source.

Thermal Energy Storage (TES) systems appear as the main solution to the abovementioned limitation, as they can store the excess energy harnessed during the day for use during the night. Latent heat storage (LHS) is one of the mechanisms that can be implemented by TES systems, in which heat is stored during the phase-change process of the storage medium as latent heat. These storage mediums are called phase change materials (PCM) and several studies on its implementation in solar domestic hot water (SDHW) systems can be found in the literature. Despite the numerous advantages of PCMs, they

share an inconvenient common trait: their thermal conductivity is fairly low, leading to low heat transfer rates.

The incorporation of PCMs in heat exchangers (HE) could prove to be an efficient solution to these materials' unfavorable thermal property, as these are systems that aim to increase the heat transfer between two or more media.

The purpose of this master's thesis is to develop a numerical model of a system for domestic hot water implementation aiming to reduce electricity consumption for water heating, and consequently reducing the carbon footprint. In order to do that, a solar water heating system (composed by a PVT flat plate, a storage tank and a plate heat exchanger (PHE) with integrated PCM) will be modeled in Simulink/MatLab. Different configurations for both the system and the PHE will be tested and the behavior of the system will be analyzed for different climatic conditions. In addition, three PCMs will be considered, and their behavior will be compared under the same conditions. Finally, the selected system and PCM will be tested under the climatic conditions of three different locations in Portugal, and its performance will be assessed.

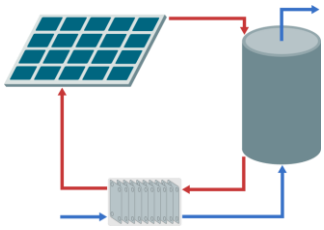

Figure 1 - Schematic of the SDHW system.

2. STATE OF THE ART

Solar energy systems have shown a great potential and have attracted great interest from researchers and manufacturers around the world, due to its abundance and economical and environmental benefits. Solar energy systems may be divided into two main groups: photovoltaic (PV) systems and solar thermal systems. Solar PV systems are used to convert radiation from the sun, in the form of light, to electrical energy by using thin films of solar cells. Solar thermal systems apply several technologies to harness solar energy in the form of heat.

Generally, only around 15%-18% of the solar radiation incident on a PV module is converted into electrical power, while the rest causes over-heating of the solar cell [3], which raises two major problems: electrical efficiency reduction and PV module damage. Hybrid photovoltaic/thermal (PVT) systems (a combination of the two named above) arise as a solution to overcome the overheating problems, as well as to improve the overall efficiency of the solar system, by removing the heat from the solar cells and using it to heat up a transfer fluid (usually air or water). Consequently, PVT systems are able to produce both electricity and thermal energy.

PVT flat plate solar collectors (FPSC) are the most commonly used systems for domestic purposes, like hot water production [4]. They generally consist of a glass cover, a PV panel (with the photovoltaic cells), an absorbing flat plate (usually made of metal: copper or aluminum), the flow channels (in which the heat transfer fluid runs) and an insulator layer (see Figure 2).

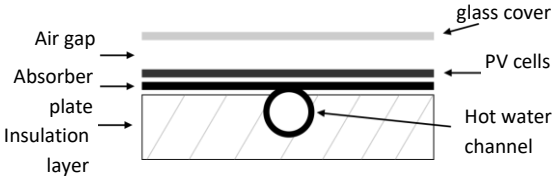

Figure 2 - Schematic of a typical PVT panel.

One of the main drawbacks of using solar energy to heat domestic water is the mismatch between energy supply and demand periods. To tackle this issue, TES systems may be implemented in SDHW systems. This technology allows the storage of excess energy, so that the energy can be used when needed. TES comprises a multitude of technologies based on three mechanisms of heat transfer: sensible heat, latent heat and thermochemical reactions.

PCMs are used for LHS. These materials store excess heat during the phase change process, which presents two benefits: the process yields a higher energy density than sensible heat storage (SHS), requiring a smaller volume, while also being able to store heat for a longer period of time. The selection of a PCM for a certain application must take into account several aspects such as its melting point, latent heat of fusion, thermal expansion, density, thermal conductivity, and material compatibility. Based on the material's nature, PCMs may be divided in three main categories: organic materials (paraffin and non-paraffin), inorganic materials (salt hydrates and metallics) and eutectic materials. However, these materials present an important disadvantage, which is their low thermal conductivity, leading to low heat transfer rates. Therefore, PCMs are usually coupled with methods that aim to improve heat transfer.

An efficient way to enhance the heat transfer between two or more mediums is through the use of a HE. PHEs are considered a compact type of HE, due to their large heat transfer area to

volume ratio, requiring a lesser volume for the equipment. PHEs occupy around 80% less floor space, when compared to shell and tube HEs [5]. They can be divided into four main categories, these being brazed, welded, semi-welded and gasketed. This last one essentially consists of a series of thin rectangular plates, where the heat transfer occurs, sealed around its edges by gaskets and held together by a frame. Each plate has typically four portholes in order to allow the passage of two different fluid stream flows (see Figure 3).

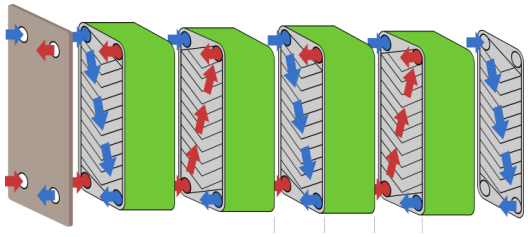

Figure 3 - Schematic of a PHE with PCM intercalated between a hot and a cold water channel.

These HEs present several advantages when compared to others. They have a great flexibility, allowing for easy inspections and cleaning of the device. The turbulent flow induced by the corrugations of the plates coupled with a high area to volume ratio provide high heat transfer rates, which leads to better efficiencies. Up to 90% of the heat can be recovered, whereas for shell-and-tube, values are around 50%. Finally, the production of PHEs can be relatively inexpensive, since the plate can be pressed (or glued) together, rather than welded. However, these systems usually present high pressure drops associated with the corrugated plates and the small space between them, increasing pumping costs [5].

3. METHODOLOGY

3.1 PHE parameters

The components of the PHEs of most importance for the simulations are the chevron corrugated plates (where the heat transfer takes place). The chosen plates' width (W_{phe}) is 0.23 [m] and three different lengths (L_{phe}) were tested, these being 0.43 [m], 0.83 [m] and 1.23 [m]. Since the port diameter (D_p) considered is 0.03 [m], the effective width (W) and lengths (L) for heat transfer purposes are 0.2 [m] and 0.4 [m], 0.8[m] and 1.2[m] respectively. The chosen corrugated angle (β_p) is 45º and the enlargement factor of the plate (ϕ), which is the ratio between the plate effective heat transfer area and the plate designed area, is considered to be 1.20 (see Figure 4).

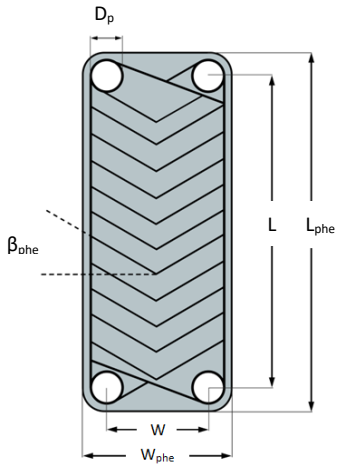

Figure 4 - PHE chevron plate.

A conventional PHE unit would present channels with hot water flow intercalated with cold water flow channels (see Figure 5). In order to incorporate the PCM within the PHE in the present work, the unit was designed as shown in Figure 6) with PCM enclosed between a hot water channel and a cold water channel.

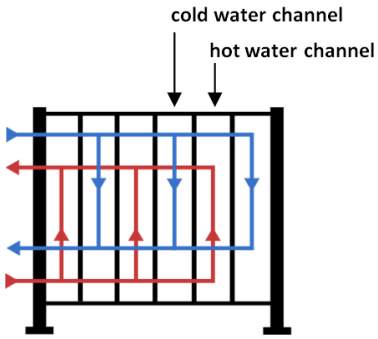

Figure 5 - Typical PHE configuration.

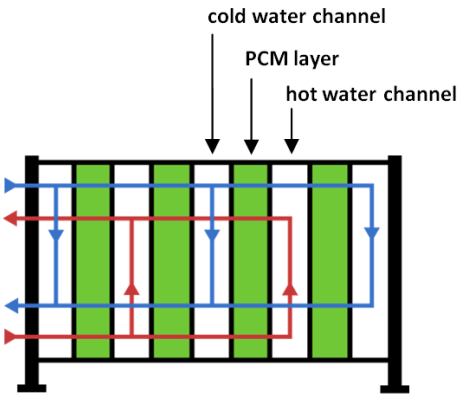

Figure 6 - Configuration of the PHE considered in this work.

The thickness of the hot water channel is 0.005 [m], while the thicknesses of the PCM layer and of the cold water channel vary for each configuration considered. Three cold water channel's thicknesses are considered, these being 0.05 [m], 0.1 [m] and 0.15[m]. The three PCM layer

thicknesses depend on the other parameters. For the PCM inside the PHE, a percentage of volume, rather than a fixed value for its thickness, is considered. Inside the PHE, the PCM volumes considered are 10%, 20% and 30% of the volume of water inside the tank (200 liters) corresponding to 20, 40 and 60 liters of PCM respectively.

3.2 Phase change material selection

In domestic hot water systems, due to the risk of contamination by Legionella, it is recommended to keep the water in the reservoir at around 60 °C, since the bacteria cannot survive at these temperatures. So, if the PCM would be placed inside the tank, PCMs with a melting range at around 60 °C should be selected. However, the PCM is to be integrated in the PHE and not inside the tank itself, and the PHE optimal temperature (the temperature to which the water inside the PHE should be preheated in order to lead to the lowest electrical costs) is not known. Therefore, a wider range of temperatures should be taken into account. Since the purpose of the PHE is to preheat the water that enters the tank, the water inside the PHE should have a lower temperature than that of the tank. So PCMs were chosen as to cover a melting range from around 50 °C to 60 °C.

Three different PCMs have been selected. Two of them inorganic (SP50 and SP58) and the remaining one organic (RT54HC). Table 1 presents some of the thermal properties of these materials.

Table 1 - Thermal properties of the PCMs.

	Melting Area (°C)	Heat Storage Capacity (kJ/kg)	Thermal Conductivity (W/m.K)
SP50	50 - 51	220	0.6
RT54HC	53 - 54	200	0.2
SP58	56 - 59	250	0.6

3.3 PVT solar panel parameters

In this work, a PVT panel was projected to produce both electricity and domestic hot water to be used by a family of four throughout the day. The system is composed by a glass cover, an air gap, a layer of PV cells, an absorber plate, the hot water channels, and an insulation layer, as seen in Figure 2.

With regard to the PV cells, crystalline silicone (c-Si) was the selected material, this being the prevailing technology available in the market for the production of the PV panel. This provides a better electrical efficiency when compared to thin-film technologies, despite its cells' higher thickness [6]. Concerning the configuration of the channels where the HTF flows, the sheet-and-tube is the most promising one, due its low production cost, whilst being only slightly less efficient than other alternatives [7].

The panel was assumed to be facing south, with an inclination (β) of 45º and a total surface area of 6 m². The absorber tubes (20 were considered), where the heat transfer fluid flows, are 3 [m] long and have an internal diameter of 0.008 [m].

3.4 Tank parameters

A water storage tank with a mantle heat exchanger was modeled. The model consists of a tank, a mantle heat exchanger, and an insulation cover. The hot water stream flows through the mantle, while the cold water stream is stored inside the tank. A tank of 200 liters of volume was considered, with a height of 1.2 [m] and a diameter of 0.46 [m]. The annulus-shaped mantle (welded around the tank) has an outer diameter of 0.50 [m], and the same height of the tank (1.2 [m]). The insulation layer covering the totality of this subsystem has a thickness of 0.03 m (see Figure 7).

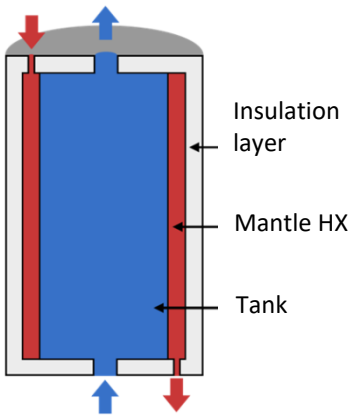

Figure 7 - Water storage tank.

3.5 PHE model

For the heat exchanger model, the lumped parameter approach was implemented. The model was developed discretizing this subsystem into thermal nodes through both the x and y directions (see Figure 8). The heat exchanger was divided into units of two different types (unit 1 and unit 2, as shown in Figure 8, in order to reduce simulation times. Unit 1 simulates the behavior of the layers in the middle of the PHE, and unit 2 simulates the behavior of the layers at the ends of the PHE.

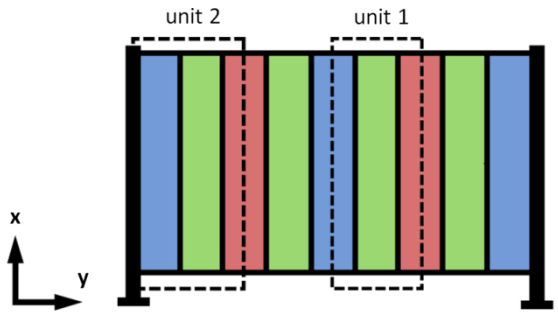

Figure 8 - Division of the PHE model into two units.

Part of a unit 1 is shown in Figure 9(a). Only half of the thickness of each of the water streams is considered for the unit's numerical model, given the symmetry of the heat exchanger in the x direction (the other half is under similar conditions, so the results could be extended to it). In Figure 9(b) is illustrated part of a unit 2, which is similar to unit 1, except that the whole thickness of the cold water channel is taken into account, as well as the losses to the exterior.

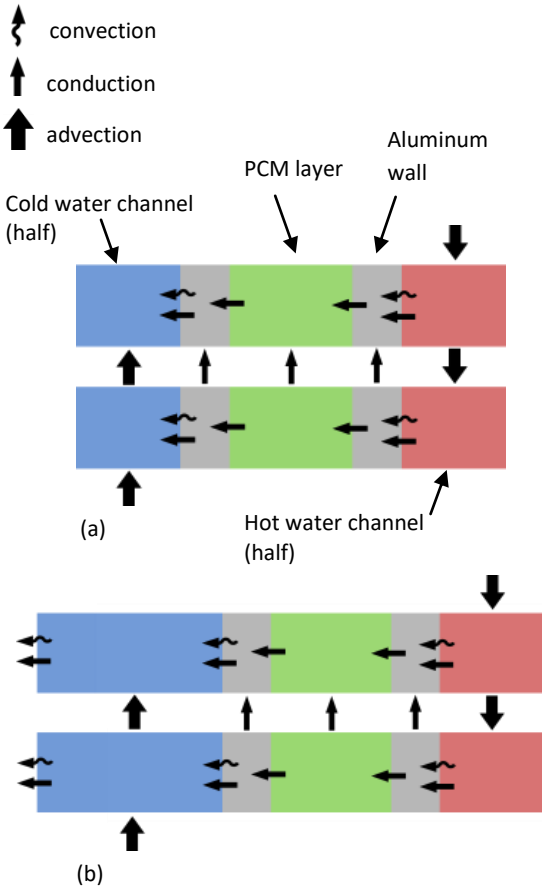

Figure 9 - Unit 1 (a) and Unit 2 (b).

Due to the large number of equations necessary to describe the system, only one is shown below as an example (see Equation 1). The equation presents the heat balance of a hot water node, which takes conduction, convection and advection into account.

$$\rho_{a1} Cp_{a1} V_{a1} \frac{dT_{a1,i}}{dt} = \frac{(T_{p1,i} - T_{a1,i})}{R_{p1}} + \\ + \dot{m}_{a1} \,.\, Cp_{a1}\left(T_{a1,i-1} - T_{a1,i}\right) \quad (1)$$

3.6 Apparent heat capacity method

To model the phase change of the PCM, this method employs an apparent increase of the storage medium's heat capacity values for the temperature range where phase change occurs. This increase corresponds, consequently, to the absorption/release of latent heat.

3.7 PVT solar panel model

The lumped parameter approach was used to model the PVT panel as well. A 1-D model was developed to discretize the PVT panel into five thermal nodes excluding the water inside the channels (6), which was modeled the same way as the water in the HE. The five thermal nodes correspond to the glass cover (1), the air gap (2), the PV cells (3), the absorber plate (4) and the insulation layer (5) (see Figure 10).

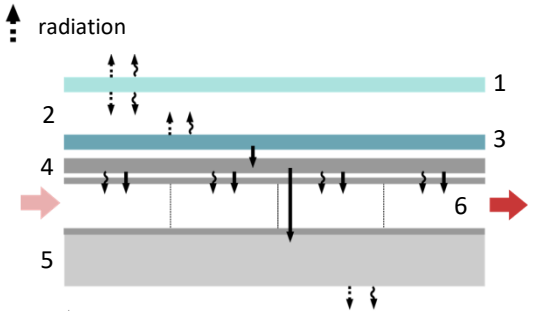

Figure 10 - PVT model.

Similarly to before, only one equation is shown below as an example (see Equation 2). The equation presents the heat balance on the insulation layer, which takes conduction, convection, and radiation into account.

$$\rho_{iso} Cp_{iso} V_{iso} \frac{dT_{iso}}{dt} = \frac{(T_{abs} - T_{iso})}{R_{abs-iso}} + \\ + h_{c_{iso-amb}} \,.\, A_{pvt}(T_{amb} - T_{iso}) + \\ + h_{r_{iso-s}} \,.\, A_{pvt}\left(T_{sky} - T_{iso}\right) \quad (2)$$

3.8 Tank model

Lastly, the tank model is presented. As in the previous subsystem, the lumped parameter approach was applied. Similarly to the PHE model, a discretization of this subsystem into thermal nodes through both the x and y directions was performed (see Figure 11). In order to reduce

simulation times, due to the symmetry of the model in the y direction, only half of the tank is considered for the numerical model.

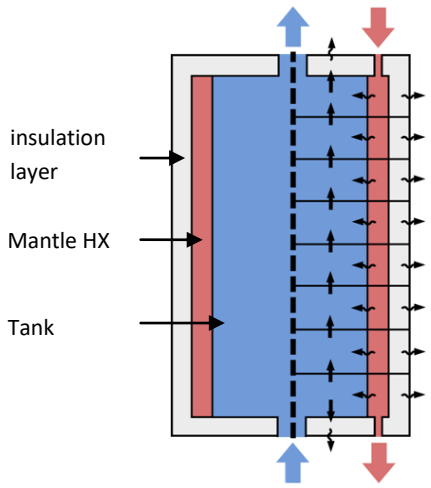

Figure 11 - Tank model

One equation is shown below as an example (see Equation 3). The equation presents the heat balance on a mantle node, which takes conduction and convection into account.

$$\rho_{ma} Cp_{ma} V_{ma} \frac{dT_{ma}}{dt} = \\ = \dot{m}_{ma} \cdot Cp_{ma}\left(T_{ma,i-1} - T_{ma,i}\right) + \\ + U_{t-ma} \cdot A_t\left(T_{t,i} - T_{ma,i}\right) + \\ + U_{ma-ext} \cdot A_{ma-ext}\left(T_{amb} - T_{ma,i}\right) \quad (3)$$

3.9 Climatic data

The numerical simulations were run for three different areas of Portugal (Lisboa, Castelo Branco, and Montalegre), and for two distinct days, one in the winter (first of January) and one in the summer (first of July). The three locations were chosen so that all climatic regions (for summer and for winter) were represented in this study. Hourly values for solar radiation, wind velocity and ambient temperature were obtained from a program provided by LNEG.

3.10 Hot and cold water streams

The mass flow rate of the hot water stream is considered 0.02 [kg/s] (typical flow rate for the heat transfer fluid). Due to the radiation from the sun only being available from 6 a.m. to 18 p.m. (roughly, although it depends on the day of the year), the pump for the solar panel stream only works during this period.

The mass flow rate of the cold water stream is only running during consumption. Three moments were considered for the consumption of DHW: two baths in the morning (one soon after the other, starting at around 6:45), two baths at night (again, one right after the other, starting at around 21:00) and washing the dishes after dinner (at around 22:30). Typical values for the volumetric flow rates for the baths and the dishwashing are 9 [l/min] and 5 [l/min] respectively (which correspond to around 0.13174 [kg/s] and 0.06587 [kg/s] respectively).

4. RESULTS AND DISCUSSION

The first step was to determine the parameters of the PHE that provide the best performance. This procedure was followed for the two system configurations (SC1 and SC2) and for the two days chosen for this study (one in the winter and one in the summer). This selection was done solely with climatic data for Lisboa, to reduce simulating times. With these results, the most suitable SC was selected. Then, the selection of the PCM was performed. Finally, with all the parameters and the PCM selected, simulations were carried out for the three locations: Lisboa, Castelo Branco, and Montalegre.

First, the thickness of the cold water channel was selected, followed by the selection of the number of layers. Then, the length of the PHE layers was defined and finally, the thickness of the PCM layer. The values considered for each of the four parameters are summarized, for facilitation purposes, on Tables 2 and 3 (for SC1) and 4 and 5 (for SC2), for the two days considered).

Table 2 - PHE parameters for SC1 (July).

	July			
Cold water thick	0.05	0.1	0.15	
N^{er} of PCM layers	6	8	10	12
Length	0.4	0.8	1.2	
PCM thick	0.016	0.031	0.047	

Table 3 - PHE parameters for SC1 (January).

	January			
Cold water thick	0.05	0.1	0.15	
N^{er} of PCM layers	6	8	10	12
Length	0.4	0.8	1.2	
PCM thick	0.007	0.014	0.021	

Table 4 - PHE parameters for SC2 (July).

	July			
Cold water thick	0.05	0.1	0.15	
N^{er} of PCM layers	6	8	10	12
Length	0.4	0.8	1.2	
PCM thick	0.042	0.083	0.125	

Table 5 - PHE parameters for SC2 (January).

	January			
Cold water thick	0.05	0.1	0.15	
N^{er} of PCM layers	6	8	10	12
Length	0.4	0.8	1.2	
PCM thick	0.007	0.014	0.021	

Since the purpose of this work was to develop a system that heats the DHW to the desired temperature of 60 °C inside the tank with the lowest possible electricity consumption, the criterion of selection for all the parameters was the additional electric power required to heat the DHW. Since the results from SC1 and SC2 are similar, only the graphics obtained for SC1 are presented.

For the selection of the thickness of the cold water channel of the PHE, simulations were run for the three thickness values, and its influence on the tank's water temperature was studied. For SC1 (July), evolution of the temperature of the water inside the tank throughout the day, for each thickness, is shown in Figure 12.

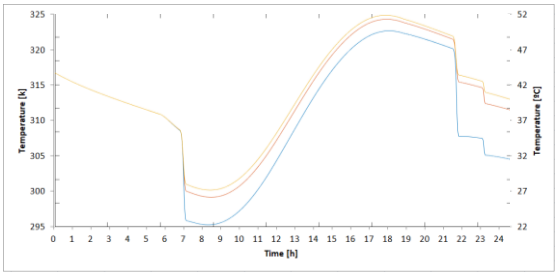

Figure 12 - Evolution of the temperature of the water inside the tank for SC1 (July), for each thickness of the cold water channel. Thicknesses: 0.05 [m] (blue), 0.1 [m] (orange) and 0.15 [m] (yellow).

From the beginning of the day until 6:00 the tank is only losing heat to its surroundings. At 6:00, when the hot water starts to flow, it is yet relatively colder than the water inside the tank (it did not have time to heat up enough yet), so the tank starts losing heat to the hot water stream as well, which is represented by a steeper decline. At 6:45 (time considered for the start of the first bath), hot water is withdrawn from the tank, while preheated water from the PHE enters the tank. This is represented by a sharp decrease in the tank's water temperature. From 8:00 to 17:30 the temperature of the hot water stream (which is heated by the sun) is finally larger than the temperature of the water inside the tank, which begins to be heated, reaching a peak at 17:30. At that point, the hot water stream is again colder than the water inside the tank and the temperature starts to decrease. From 18:15 until the end of the day, the hot water stream stops running, and the tank is once again only losing heat to its surroundings. The second series of baths takes place at 21:00, represented by a sharp decrease in the tank's water temperature, followed by another sharp decrease at 22:30, corresponding to the use of hot water to wash the dishes, following the same behavior as in the first series of baths.

Temperature decrease during hot water consumption (at 6:45, 21:00 and 22:30) is smaller for the configuration with a larger thickness of the channel of cold water, and more pronounced for the one with smaller thickness. Despite this, during the temperature rise from 8:00 to 17:30, the configuration with a smaller thickness shows the highest relative rise in the tank's water temperature. The relatively less pronounced rise in temperature (from 8:00 to 17:30) of the configuration with a larger thickness is compensated by a much lesser decrease while hot water is being used, providing a better overall system performance.

This behavior is the same for July and January, for both SCs.

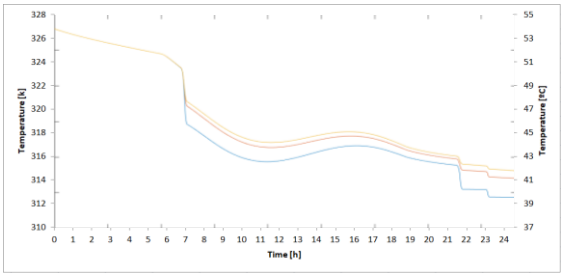

Figure 13 - Evolution of the temperature of the water inside the tank for SC1 (January), for each thickness of the cold water channel Thicknesses: 0.05 [m] (blue), 0.1 [m] (orange) and 0.15 [m] (yellow).

The graphic obtained for January presents a similar behavior as the one for July, the main difference being the temperature rise during sun exposure, which is much smaller for January.

The same procedure was followed for the selection of the number of layers. Evolution of the water temperature inside the tank for SC1 is presented in Figure 14 (for July) and Figure 15 for January). The graphics obtained are similar to the ones obtained before.

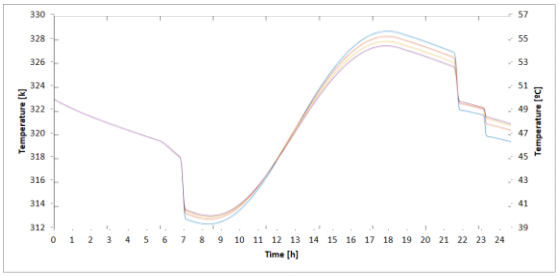

Figure 14 - Evolution of the temperature of the water inside the tank for SC1 (July), for each number of layers considered. Number of PCM layers: 6 (blue), 8 (orange), 10 (yellow) and 12 (purple).

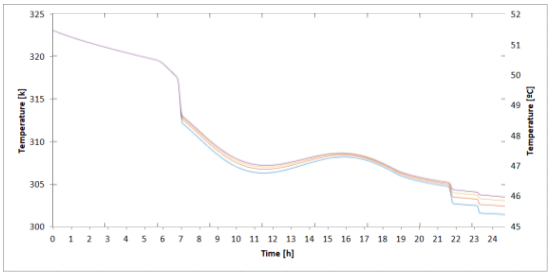

Figure 15 - Evolution of the temperature of the water inside the tank for SC1 (January), for each number of layers considered. Number of PCM layers: 6 (blue), 8 (orange), 10 (yellow) and 12 (purple).

For July, the configuration that led to the lowest electricity consumption was the one with 8 layers of PCM, while for January was the one with 12 layers of PCM. Similar results were obtained for SC2, where, for July, the configuration that presented the best performance was the one with 6 layers of PCM, while for January was again the one with 12 layers.

For the selection of the length of the layers, simulations were run for the three lengths presented before. The behavior of the water temperature inside the tank is analyzed (Figure 16 and Figure 17).

Once again, the temperature of the water inside the tank presented similar behaviors to the ones previously observed. For July, the PHE with a length of 0.8 m was the one that presented the best results, while for January PHE with the widest layers was the one that presented the best performance. As for the previous parameters, SC2 presented similar results, with the lengths of the PHE layers presenting the best performance being 0.4 m and 1.2 m for July and January respectively.

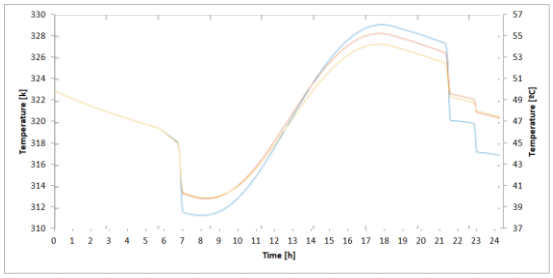

Figure 16 - Evolution of the temperature of the water inside the tank for SC1 (July), for each length of the PHE layers. Lengths: 0.4 [m] (blue), 0.8 [m] (orange) and 1.2 [m] (yellow).

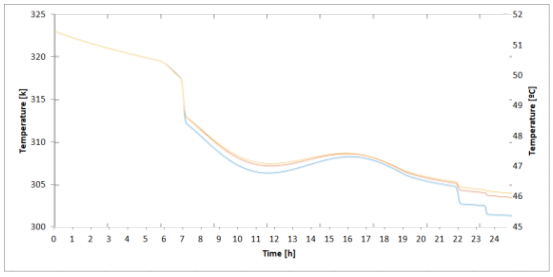

Figure 17 - Evolution of the temperature of the water inside the tank for SC1 (January), for each length of the PHE layers. Lengths: 0.4 [m] (blue), 0.8 [m] (orange) and 1.2 [m] (yellow).

The final parameter of the PHE to be studied on this thesis was the thickness of the PCM layer.

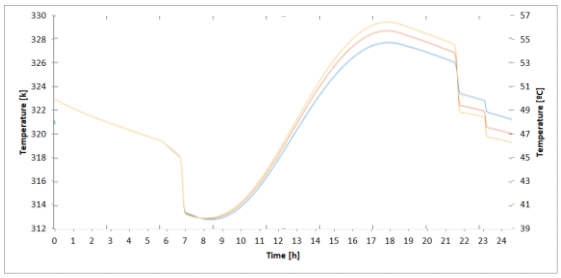

Figure 18 - Evolution of the temperature of the water inside the tank for SC1 (July), for each thickness of the PCM layer. Thicknesses: 0.016 [m] (blue), 0.031 [m] (orange) and 0.047 [m] (yellow).

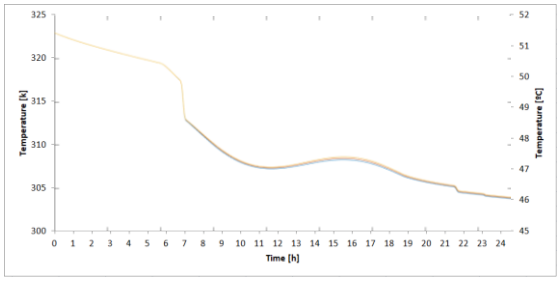

Figure 19 - Evolution of the temperature of the water inside the tank for SC1 (January), for each thickness of the PCM layer. Thicknesses: 0.007 [m] (blue), 0.014 [m] (orange) and 0.021 [m] (yellow).

Here, similarly to the thickness of the cold water layer, the thickness of the PCM layer that presented the best results was the largest one, for both SCs and both days of the year.

After the selection of the parameters of the PHE, we got the four PHE configurations that presented the best performances: one for SC1 optimized for January, one for SC1 optimized for July, and the same for SC2. Of these four, only one could be selected (since, in practice, the user will not be changing the PHE settings depending on the day of the year). Comparing the four configurations, the one that led to the lowest electricity consumption was the PHE configuration of SC1 optimized for July.

With the configuration selected, simulations were carried out to test the three PCMs considered: SP50, RT54HC and SP58. RT54HC has a much lower thermal conduction than the other two PCMs, not being able to absorb as much heat. Due to this fact, for July, while the entire volume of the other two PCMs enters phase change, a portion of RT54HC remains in the solid phase, and the temperature of the water inside the PHE does not heat up as much. However, the simulations with RT54HC led to less electricity required to heat the water inside the tank to 60 °C. Therefore, RT54HC was the selected PCM to carry the simulations for the three locations.

After all the parameters, SC and PCM were selected, simulations were run for the three locations selected beforehand: Lisboa, Castelo Branco, and Montalegre. To assess the improvement in the system's performance, the evolution of the temperature of the water inside the tank is shown for all three locations, for both the systems with and without the PHE.

The improvements due to the introduction of the PHE in the system are evident during the consumption of hot water for the three locations, for both July and January.

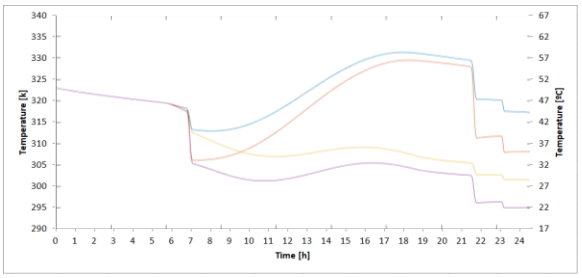

Figure 20 - Evolution of the temperature of the water inside the tank with (blue and yellow) and without (orange and purple) PHE for July and January respectively (Lisboa).

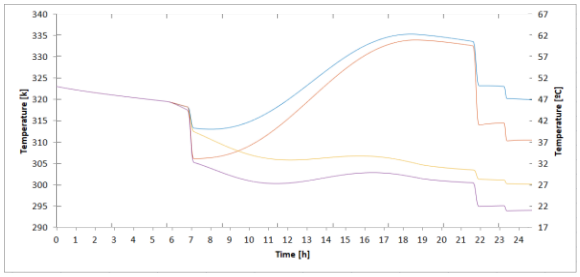

Figure 21 - Evolution of the temperature of the water inside the tank with (blue and yellow) and without (orange and purple) PHE for July and January respectively (Castelo Branco).

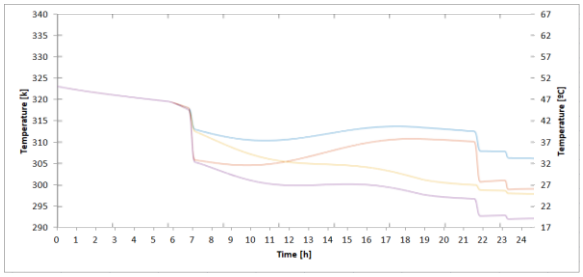

Figure 22 - Evolution of the temperature of the water inside the tank with (blue and yellow) and without (orange and purple) PHE for July and January respectively (Montalegre).

The preheated water fed by the PHE to the tank is at a much higher temperature than the one that comes directly from the external supply. Therefore, the system with the PHE provides much lower temperature drops at 6:45, 21:00 and 22:30 (when water from the cold stream enters the tank).

For January, the improvements due to the introduction of the PHE are similar for the three locations considered. However, for July, the performance enhancement is significantly lower for Montalegre than for the other two locations. This may be due to the fact that, during summer, the temperatures reached in this region are not enough to initiate phase change on the PCM, unlike for the other two. The systems incorporating the PHE presented better results for all three locations. The energy requirements to keep the water inside the tank at 60 °C are given in Tables 6, 7, and 8.

Table 6 - Energy (kJ) required to keep the water inside the tank at 60 °C (Lisboa).

	Lisboa	
	PHE	**No PHE**
July	7.816×10^4	10.15×10^4
January	15.79×10^4	18.3×10^4

Table 7 - Energy (kJ) required to keep the water inside the tank at 60 °C (Castelo Branco).

	Castelo Branco	
	PHE	**No PHE**
July	6.676×10^4	8.934×10^4
January	16.58×10^4	19.1×10^4

Table 8 - Energy (kJ) required to keep the water inside the tank at 60 °C (Montalegre).

	Montalegre	
	PHE	**No PHE**
July	13.63×10^4	16.07×10^4
January	17.51×10^4	20.06×10^4

5. CONCLUSION

This thesis was developed with two main objectives: to study the performance and the behavior of a PHE with the incorporation of PCM and to study the efficacy and influence of such a system as a preheater in a SDHW system.

The models for the three different subsystems which compose the hybrid solar PVT energy storage system for a residential house were developed and implemented in Simulink/MatLab. Simulations were run for several different scenarios (to take into account different climatic conditions) and configurations, and the analysis of the results was performed. When compared to the same system without the incorporation of the PHE, the developed system showed a potential of reducing electricity consumption by around 23% for summer, and 14% for winter for the Lisbon simulations.

The PHE HE type was chosen due its high area/volume ratio, in order to try to counteract the PCM's low conductivity. This shows good results for when the cold water stream is not running (since there is no consumption). However, when the cold water stream is running, the PHE's area/volume ratio is not high enough to compensate for the poor conductivity of the PCM. This happens because the residence time of the cold water inside the PHE is too short for the cold water to heat up sufficiently. Other heat transfer enhancement techniques might prove useful to tackle this issue.

REFERENCES

[1] REN21 Members. "Renewables 2019 Global Status Report". 2019. Available: https://wedocs.unep.org/bitstream/handle/20.500.11822/28496/REN2019.pdf?sequence=1&isAllowed=y%0A.

[2] O. A. Rehman. "Integration of solar domestic hot water system with thermal energy storage based on phase change materials". Instituto Superior Técnico, Lisboa, Portugal, 2019.

[3] M. C. Browne, B. Norton and S. J. McCormack. "Heat retention of a photovoltaic/thermal collector with PCM". *Solar Energy*, 133: 533-548, 2016.

[4] M. Hamed, A. Fellah and A. B. Brahim. "Parametric sensitivity studies on the performance of a flat plate solar collector in transient behaviour". *Energy Conversion and Management*, 78: 938-947, 2014.

[5] S. N. Kazi. "Heat Transfer Studies and Applications". AvE4EvA MuViMix Records, 2015.

[6] N. Aste, C. Del Pero and F. Leonforte. "Water flat plate PV-thermal collectors: A review". *Solar Energy*, 102: 98-115, 2014.

[7] R. M. da Silva and J. L. M. Fernandes. "Hybrid photovoltaic/thermal (PV/T) solar systems simulation with Simulink/Matlab". *Solar Energy*, 84: 1985-1996, 2010.